URN (Paper): urn:nbn:de:gbv:ilm1-2011iwk-024:6

56TH INTERNATIONAL SCIENTIFIC COLLOQUIUM
Ilmenau University of Technology, 12 – 16 September 2011
URN: urn:nbn:gbv:ilm1-2011iwk:5

# TRANSVERSAL VIBRATIONS OF BEAMS WITH BOUNDARY DAMPING IN THE CONTEXT OF ANIMAL VIBRISSAE

*Micha Schaefer / Tonia Schmitz / Christoph Will / Carsten Behn*

Department of Technical Mechanics
Ilmenau University of Technology
Max-Planck-Ring 12 (Building F)
98693, Ilmenau, Germany
{Micha.Schaefer, Christoph.Will, Carsten.Behn}@tu-ilmenau.de / toini@gmx.de

**ABSTRACT**

Mice and rats use a sophisticated sensory system to acquire tactile information about their surroundings. Vibrissae, located in the mystacial pad, are either used passively to sense environmental forces (e.g., wind) or actively, when they rhythmically scan objects or surfaces. Some approaches to the biological paradigm vibrissa use rigid body systems in which a rod-like vibrissa is supported by a combination of spring and damping elements modeling the viscoelastic properties of the follicle-sinus-complex. However, these models can only offer limited information about the functionality of the biological sensory system, as they neglect its determining property: the inherent elasticity of the tactile hair. To increase the accuracy and the applicability of the gathered information, the vibrissa is modeled as an elastic beam in this paper. The classical differential equation (derived from the Euler-Bernoulli-equations) is applied to vibrissa beam models with varying supports using discrete and continuously distributed spring and damping elements. The eigenfrequency spectrum of such beams are being determined analytically and numerically, while varying the viscoelastic properties of the support.

***Index Terms—*** vibrissa, elastic beam, Euler-Bernoulli-equation, discrete viscoelastic support, follicle-sinus-complex, eigenfrequencies.

## 1. INTRODUCTION

### 1.1. The biological paradigm

Starting point and background of this work are the mystacial vibrissae — a complex **tactile sensory organ** which complements the visual and aural sensing in a large number of nocturnal animals. The functionality of these vibrissae vary from animal to animal and is best developed in rodents, especially in mouses and rats, [1], see Fig. 1.

**Fig. 1**. Mammals with vibrissae: a cat (left, [2]), and a rat (right, [3]).

The mystacial vibrissae are arranged in an array of columns and rows around the snout, see Fig. 2.

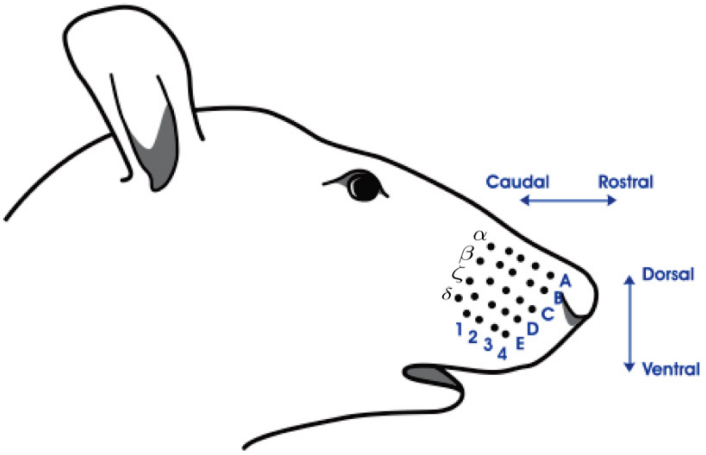


**Fig. 2**. Schematic drawing of the mystacial pad, [4].

Similar to ordinary hairs, vibrissae are made out of dead material, although in contrast to these, the tactile hair is stiffer and has a hollow conical shape, [4]. Each vibrissa is embedded in a follicle-sinus-complex (FSC), see Fig. 3, assuring its viscoelastic support, [5].

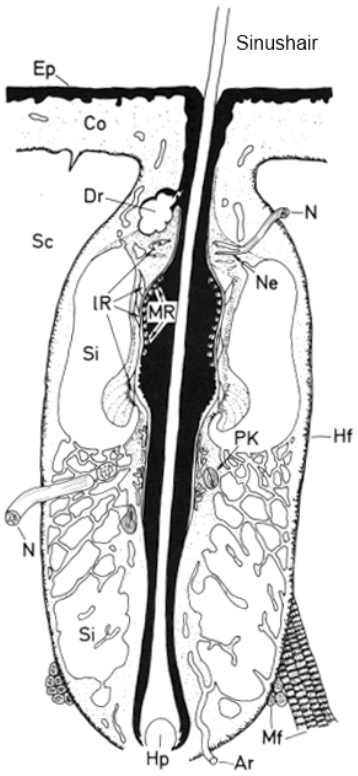


**Fig. 3**. FSC of a vibrissa, [6].

The FSC is characterized by its exceptional arrangement of blood vessels, neural bonding and muscles. It is assumed that the rodents can control the viscoelastic properties of the vibrissa's support by regulating the blood supply to the sinus (Si, likewise a blood sac), [5], [4]. The nerves (MR, IR), stimulated by deflections of the hair, transmit the information through several processing units to the central nervous system (CNS).
The musculature is divided in extrinsic and intrinsic musculature. By activating the first one the whole tuft of vibrissae can be moved. In contrast, the intrinsic musculature adjust the angle position and the motion of a single vibrissa. The contraction of the intrinsic musculature moves the FSC backwards and therefore the sinus hair forward,

[7], [6].
This enables rodents to use their vibrissae in two different ways:

- In the **passive mode**, the vibrissae are being deflected by external forces (e.g., wind). They return to their rest position passively — thus without any muscle activation.

- In the **active mode**, the vibrissae are swung back- and forward by alternate contractions of the intrinsic and extrinsic muscles, see Fig. 4.

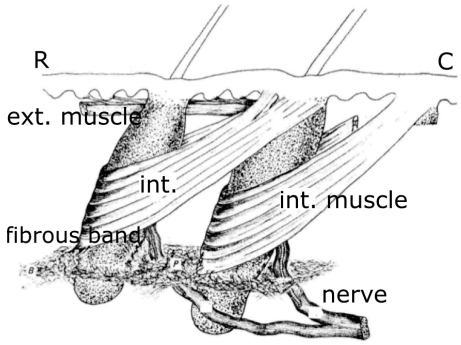


**Fig. 4**. Schematic drawing of two neighboring mystacial follicles, which can be moved by extrinsic and intrinsic muscles (latter innervated by the facial nerve). Note that the attachment point of an intrinsic muscle sling is always situated at its neighboring follicle. (R - rostral, C-caudal) [5].

By contracting the **extrinsic musculature**, the whole mystacial pad (snout region) is being moved backward. In contrast, the contraction of an **intrinsic muscle-sling**, leads to the protraction of just one single vibrissa, [5], [6]. By adjusting the frequency and amplitude of the oscillations, the rodents are able to investigate object surfaces and shapes amazingly fast and with high precision, [8].

### 1.2. Mechanical models of the vibrissa

In order to analyze the mechanical and especially the dynamical behavior of the vibrissa, the physical principles of the paradigm have to be identified. Therefore abstract technical models, which describe the biological example in detail and are suitable to be analyzed using engineering and scientific methods, are sought.
Usually two types of models are used to analyze the mechanical behavior of the vibrissa:

- **Rigid body models** consider the vibrissa as a steep, inelastic body. Such models have the advantage of a simple mathematical description and solution. Furthermore, these models can easily be used to analyze the influence of varying viscoelastic supports, [9]. However, neglecting the inherent elasticity of the vibrissa implies a questionable oversimplification of the biological example.

- **Continuum models** are closer to the biological paradigm, as the tactile hair is implemented as an elastic beam. They are thus able to take into account the inherent dynamical behavior and the bending stiffness of the biological vibrissa. Further on, the influence of the conical vs. cylindrical shape of the hair can be investigated on the basis of these models, see [10].

**Example 1.1.** *Figure 5 presents an example of a complex single vibrissa model in the mystacial pad. The tactile hair is modeled as an elastic beam, the U-frame marks the rigid wrapping of the FSC. The viscoelastic properties of the blood-sinus are taken into account by (controllable) spring and damping elements. Further on, the embedding of the FSC in the skin and the coupling of the vibrissa in the mystacial pad by the intrinsic and extrinsic musculature is realized by spring and damping elements.* ◇

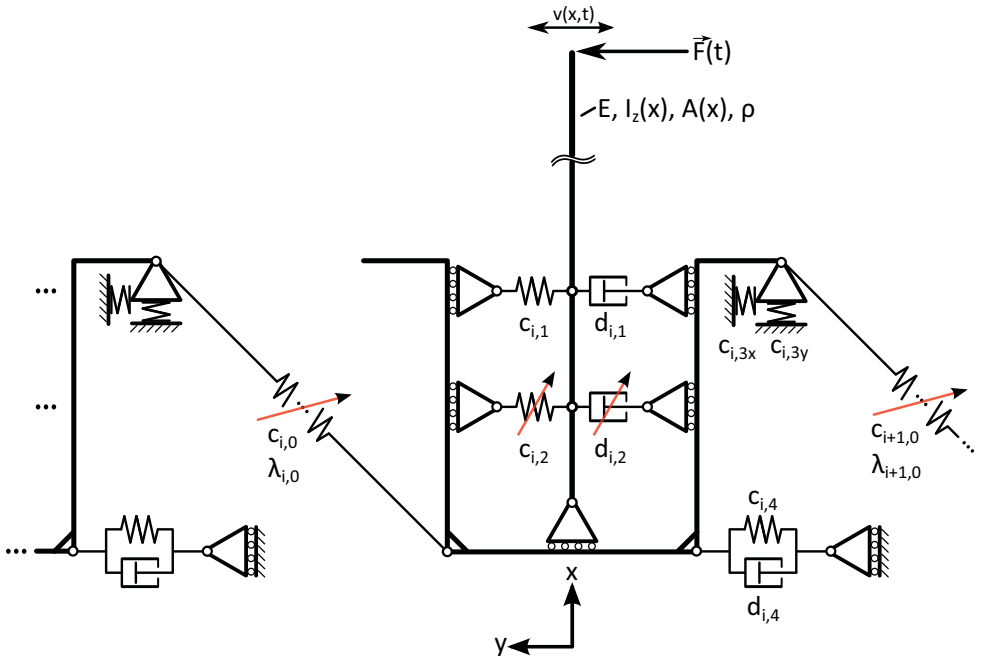


**Fig. 5**. Example of a vibrissa model

### 1.3. State of the art

An intensive literature overview of technical vibrissa models (rigid body and continuum) has been presented in [9]. The following summarizing tables present the essential assertions made for the encountered mechanical models.

**Rigid body models of a vibrissa:**

- **Mitchinson (2004 [11], 2007 [12]) - Model of the FSC**
  - ⊖ too complex for a technical implementation
  - ⊕ Determinantion of spring and damping coefficients for the FSC

- **Berg (2003 [13]), Hill (2008 [14]) - Model of the musculature in the mystacial pad**
  - ⊕ Implementation of the intrinsic and extrinsic musculature
  - ⊕ Simulating the viscoelastic properties of the skin
    - ↪ Determination of spring and damping coefficients for the skin
  - ⊖ Negligence of the viscoelastic properties of the FSC
  - ⊖ Connection between the follicles
    - ↪ leads to complex control strategy and high control effort

- **Berg (2003 [13]), Hill (2008 [14]) - Determination of the range of movement of the vibrissa**
  - ↪ $\varphi_{Rest} \approx 80°$
    - angular deflection in rostral direction $\varphi_{rest} + 65°$
    - angular deflection in caudal direction $\varphi_{rest} - 35°$
    - translatory shift $\approx 5mm$ in caudal-rostral direction
    - translatory shift $\approx 3mm$ in dorsal-ventral direction

- **Schmitz (2009 [7]) - Model of the stimulus transmission**
  - ⊕ Implementation of the viscoelastic properties of the FSC, [7], [15]
  - ⊖ Negligence of the viscoelastic properties of the skin, [7], [15], [16]
  - ⊕ Simulation of the passive/active mode, [17]
    - ↪ via adaptive control algorithms

**Elastic beam models of a vibrissa:**

- **Birdwell (2007 [18]) - Model analyzing the bending behavior of nat. vibrissae**
  - ⊕ suitable to analyze the bending behavior

⊖ Linearized model: only valid for small deflections
⊕ Consideration of the conical shape of the vibrissa
⊖ Negligence of the support's compliance
⊕ Finding: Shape of the beam influences the bending behavior
↪ not negligible
⊕ Finding: Young's modulus of natural vibrissae vary

- **Birdwell (2007 [18]) - Model to determine clamping torques**
  ⊖ Linearized model only valid for small deflections
  ⊕ Consideration of the conical vibrissa shape
  ⊖ Negligence of the support's compliance
  ⊕ Finding: influence of the natural pre-curvature of the vibrissa is negligible

- **Scholz (2004 [19]) - Model for profile sensing with an actuated vibrissa**
  ⊕ Implementation of the active mode
  ⊖ Negligence of the support's compliance

- **Neimark (2003, [20]), Andermann (2004 [21]) - Model for the determination of the support's influence on the resonance properties of nat. vibrissae**
  ⊕ Experimental measurements of vibrissae's resonance frequencies
  ⊖ dubious results during numerical evaluations
  ↪ due to constant Young's modulus taken for all vibrissae
  ⊕ Finding: massive influence of the support on the resonance frequencies
  ⊕ Finding: topologically distributed sensitivity in the vibrissa array
  ⊕ Finding: transduction and processing of the resonance frequency provoking stimuli to the CNS
  ↪ Resonance frequencies contain relevant informations

- **TU Ilmenau, Dept. TM (2010) - Model for the determination of the support's influence on the eigenfrequencies of technical vibrissae**
  ⊖ Negligence of the conical shape of the vibrissa
  ⊕ Consideration of the support's compliance
  · at skin level
  · at the level of the FSC
  ⊕ Finding: massive influence of the support on the eigenfrequencies
  ⊕ Finding: influence of damping elements in the support
  ↪ massive for the $1^{st}$ eigenfrequency

### 1.4. Focus and aim of the paper

In this paper we focus on the mechanical properties and the dynamic behavior of the vibrissa. The processing of the stimulus and the linked analysis of different control strategies are **not** discussed here, see [7], [15] on this. Furthermore, the investigations are addressed to a single vibrissa — the interaction between the different vibrissae in the mystacial pad is not taken into account.
Starting point and motivation of this work are multiple **hypotheses** concerning the **functionality of the vibrissa**:

- The elasticity and the conical shape of the hair are relevant for the functionality of the vibrissa, [18].

- The viscoelastic properties of the support (FSC) are controlled by the blood pressure in the blood sinus, [5], [4].

- The vibrissae are excited with or close to their resonance frequencies during the active mode, [20], [21].

Following these hypotheses, the **primary goal** of this paper is:

- to investigate the influence of the elasticity and of the conical shape on the vibration characteristics of the vibrissa by analyzing its spectrum of eigenfrequencies;

- to analytically examine an innovative model of a flexible vibrissa with a viscoelastic support.

## 2. TRANSVERSE BENDING VIBRATIONS OF BEAMS

In order to consider the bending behavior of the sinus hair, the bending differential equations has to be derived. They are the basis of the following investigation and calculation. Form and complexity of the partial differential equations (PDE), describing the bending vibrations of beams, depend on the assumptions made before. Afterwards, the method of separation of variables is applied, which form a possibility to solve these equations.

### 2.1. Dynamic equations of motion

**Initial point of investigation**
In the literature (e.g., [22], [23], [24], [25]) the equations are gained in most cases by classical first order theory (considering the undeformed state of the beam) in applying the method of sections with assumption of small deflections. Theories gained from this simplifications are only valid for small deflections and deformations. Furthermore, there is no possibility to consider axial distribution.
In this paper a more general approach is chosen, where we are able to consider more realistic models of a biological vibrissa. This results in an equation of motion, which can be simplified to the well-known form of linear transverse vibration of beams with small deflections.

**Initial point of investigation** is the beam-element shown in Fig. 6. The variable $s$ is the arc length coordinate of the beam, while $x$ is the inertial-spatial coordinate.

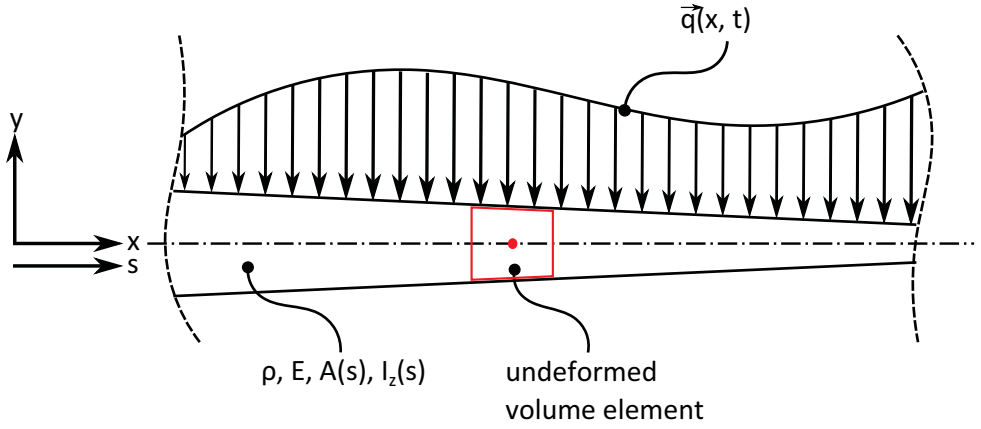


**Fig. 6**. Undeformed beam element

Under consideration of Fig. 6 the following assumptions are made:

- Only plane transverse vibrations of beams are considered.
- It is assumed that the deformations (distorsions), and therefore the inner stress, remain small besides large deflections (displacements).
- Hence, we assume: the material behaves linear-elastic and has linear damping property.

Further assumptions are:

- The centroidal axis of the undeformed beam is even.
- The beam material is homogenous an isotropic.
- Suppose that the cross-section and the load are continuously differentiable twice with respect to the arc length $s$.
- The load $\vec{q}(x,t)$ acts always parallel to the $y$-coordinate and is continuous.

If a part of the beam vibrates, every beam element (red colored) is **deformed** as well as **displaced** in $x$- and $y$-direction, see Fig. 7.

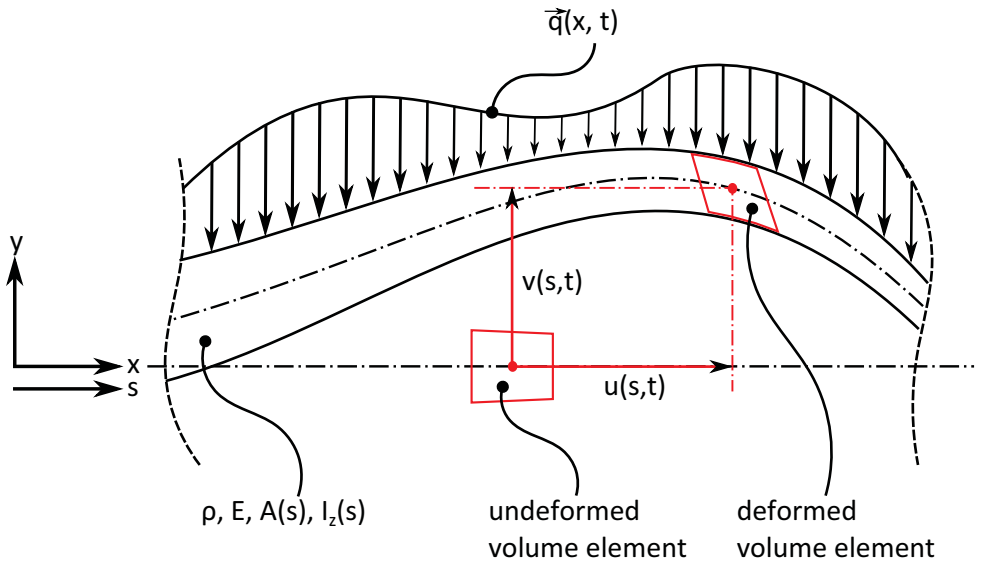


**Fig. 7**. Deformed beam element

When no torsion deformations are being considered, the total deformation is the sum of **axial-strain**, **shear-deformation** and **bending**. Under the assumption of linear material behavior, it is possible to give a relation between the inner cut quantities and the corresponding deformation ones (of a infinitesimal beam element, see Fig. 8). The geometric meaning of the deformation function can be seen in Fig. 8. Let $E$ denote Young's modulus, $G$ the shear modulus, $I_z(s)$ the second moment of area and $A(s)$ the cross-area of the beam.
Then, we get the **longitudinal elongation**:

$$N(s,t) = E\,A(s) \cdot \left( \varepsilon(s,t) + \xi \frac{\partial \varepsilon(s,t)}{\partial t} \right) \tag{1}$$

The first term, in brackets, takes the force caused by elastic deformation ($\varepsilon(s,t)$ is the longitudinal elongation) into account, and the second term the time-varying rate of deformation ($\xi$ is a material parameter).
In the same way we get for the **shear deformation**:

$$Q(s,t) = \alpha_s\, G\, A(s) \cdot \left( \gamma(s,t) + \beta \frac{\partial \gamma(s,t)}{\partial t} \right) , \tag{2}$$

where the shear angle $\gamma(s,t)$ is given by the relation $\gamma(s,t) = \phi(s,t) - \psi(s,t)$, $\alpha_s$ is a correctional factor for shear-deformation, and $\beta$ is a material damping parameter.
The **combined bending** is given by:

$$M(s,t) = E\,I_z(s) \cdot \left( \frac{\partial \psi(s,t)}{\partial s} + \tau \frac{\partial^2 \psi(s,t)}{\partial s \partial t} \right) \tag{3}$$

We note, that we use the angle $\psi(s,t)$ in case of combined bending (superposition of shear deformation) instead the pitch angle $\phi(s,t)$ due to simple bending, see [23]. Furthermore, $\tau$ equals a material damping parameter for bending.

**Formulation of the dynamic equations of motion**
In general the derive of the vibration-PDE can be done by two different ways:

- **Theory of elasticity and energy-methods:** Based on the equations of kinetic and potential energy a functional is derived using the Hamilton principle and the corresponding Lagrangean equations are determined, see [24] and [26].

- **Method of sections and applying the principles of linear and angular momentum:** An infinitesimal beam element (occurring after applying the method of sections) is considered, where the cross-sections are orthogonal to the centroidal axis. Then, the principles of linear and angular momentum are applied to this beam element, see e.g. [27], [25], [23], [22].

Here, we focus on the second method. Figure 8 shows the result of the method of sections applied on a infinitesimal beam element. Let $Q(s,t)$, $M(s,t)$, $N(s,t)$ denote the cutting quantities, explained in the last Section 2.1, $v(s,t)$, $u(s,t)$ and $\psi(s,t)$ are the motion and deflection parameters, respectively, and $s_A$, $s_I$, $s_q \in [s, s+ds]$ are points between the boundaries of the beam element.

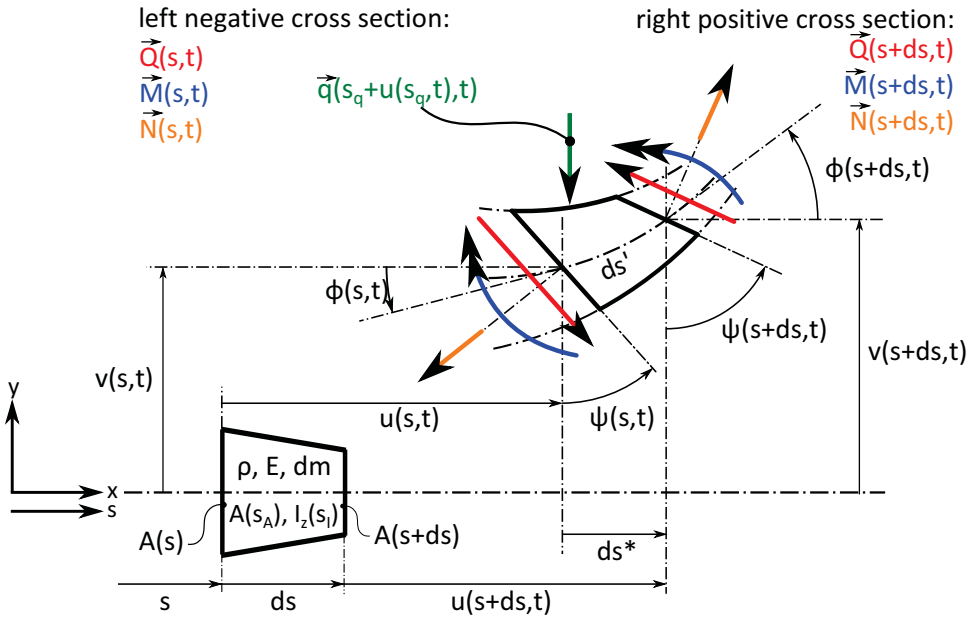


**Fig. 8**. Method of sections applied to an infinitesimal beam element

Before going into detail we state some comments on the mathematical formulation.

**Remark 2.1.** *In order to get a well arranged and compact presentation, the following notation for partial derivatives is chosen:*

$$\partial_n(\cdot) := \frac{\partial(\cdot)}{\partial n}$$

◇

**Remark 2.2.** *The formulation of the deformed centroidal axis of the beam is done in parametric representation. The following relations are used:*

$$\begin{aligned} S_x(s,t) &= s + u(s,t) \\ S_y(s,t) &= v(s,t) \end{aligned}$$

◇

**Remark 2.3.** *The following relations for slope and strain hold:*
*Slope:*

$$\tan\left(\phi(s,t)\right) = \frac{\partial_s v(s,t)}{1 + \partial_s u(s,t)}$$

*Strain:*

$$\begin{aligned} \varepsilon(s,t) &= \frac{ds' - ds}{ds} + \varepsilon_0(s) = \frac{\partial_s u(s,t) + 1}{\cos\left(\phi(s,t)\right)} - 1 + \varepsilon_0(s) \\ \textit{mit} \qquad & \varepsilon_0(s) = \frac{N_0(s)}{E\,A(s)} \end{aligned}$$

◇

**Remark 2.4.** *We conclude from the first mean value theorem for integration:*

$$\lim_{\Delta s \to 0} f(\tilde{s}) = \lim_{\Delta s \to 0} \frac{1}{\Delta s} \int_s^{s+\Delta s} f(s)\, ds = f(s)$$

◇

Due to the formulation of the centroidal axis in parametric form and the consideration of the displacement $u(s,t)$, respectively, the superposition of longitudinal and transversal bending vibrations can be determined. Setting $v(s,t) \equiv 0$ is necessary to get only longitudinal vibrations. Also $u(s,t) \equiv 0$ is a condition for transverse bending vibration only.
The principle of linear momentum formulated for each component yields — assume a time-invariant mass $m \neq m(t)$:

$$\begin{aligned} \vec{e}_x: \qquad dm(s)\,\partial_{tt}u(s,t) &= \sum_i F_{xi}(s,t) \\ \vec{e}_y: \qquad dm(s)\,\partial_{tt}v(s,t) &= \sum_i F_{yi}(s,t) \end{aligned}$$

The principle of angular momentum with respect to the center of mass — in case of constant mass moment of inertia $J_{zz} \neq J_{zz}(t)$ — is under the assumption of a rotation around one axis with fixed direction (here: $\vec{e}_z$), which is an axis of inertia):

$$\vec{e}_z: \qquad dJ_{zz}(s)\,\partial_{tt}\psi(s,t) = \sum_i M_{zi}(s,t)$$

The infinitesimal variables $dm(s)$ and $dJ_{zz}(s)$ can be substituted due to the first mean value theorem for integration as follows:

$$\begin{aligned} dm(s) &= \rho\,A(s_A)\,ds \\ dJ_{zz}(s) &= \rho\,I_z(s_I)\,ds \text{ (thin disk)} \end{aligned}$$

Taking Fig. 8 into account, the principles of linear and angular momentum can be formulated. Division of these equations by $ds \neq 0$ and applying of the limiting process $ds \to 0$ as well as the use of Remark 2.4, leads to the following system of PDEs:
**Principle of linear momentum: $x$-component**

$$\rho\,A(s)\,\partial_{tt}u(s,t) = -\partial_s\left(Q(s,t)\,\sin(\psi(s,t))\right) + \partial_s(N(s,t)\,\cos(\psi(s,t)))$$

**Principle of linear momentum: $y$-component**

$$\begin{aligned} \rho\,A(s)\,\partial_{tt}v(s,t) = \partial_s\left(Q(s,t)\,\cos(\psi(s,t))\right) + \partial_s\left(N(s,t)\,\sin(\psi(s,t))\right) \\ - q\left(s+u(s,t),t\right)\cdot\left(1+\partial_s u(s,t)\right) \end{aligned}$$

**Principle of angular momentum: $z$-component**

$$\begin{aligned} \rho\,I_z(s)\,\partial_{tt}\psi(s,t) = \partial_s M(s,t) + Q(s,t)\,\cos(\psi(s,t)-\phi(s,t))\,\frac{\partial_s u(s,t)+1}{\cos(\phi(s,t))} \\ + N(s,t)\,\sin(\psi(s,t)-\phi(s,t))\,\frac{\partial_s u(s,t)+1}{\cos(\phi(s,t))} \end{aligned}$$

Let us note the following:

- **The derived system of PDEs describes plane bending vibrations of beams under large deflection with the assumption of small deformation for the *Timoshenko beam model* — consideration of shear deformation and rotary inertia, extended by normal forces.**
- For this general case, the application of the principles of linear and angular momentum results in a system of three coupled non-linear PDEs for the motion and deformation variables $u(s,t)$, $v(s,t)$ and $\psi(s,t)$.
- The system of PDEs can not be solved exactly in an analytical way.
- The variables $\phi(s,t)$ and $\varepsilon(s,t)$ are no longer state variables. They can be calculated in using the relations from Remark 2.3.
- The cut variables $M(s,t)$, $Q(s,t)$ as well as $N(s,t)$ have to be replaced by their corresponding material relation.

As mentioned above, this system of PDEs is not suitable for further analytical investigations with respect to the goal of this paper. We have to make some additional restrictions to transform these equations of motion into more manageable ones. Then, an easier and analytic exact solvable system can be derived.
At first, the Timoshenko beam model is changed to the Euler-Bernoulli beam one, so that the effect of shear deformation and rotary inertia is disregarded. This simplification is feasible for slim beams like vibrissae. This changeover to the shear-rigid beam is given — under consideration of relation (2):

$$\begin{aligned} G\,A(s) &\rightarrow \infty \text{ (shear-rigid beam)} \\ \curvearrowright \psi(s,t) &\rightarrow \phi(s,t) \end{aligned}$$

Negligence of the rotary inertia means in terms:

$$\rho\, I_z(s,t) \rightarrow 0 \text{ (no rotary inertia)}$$

These equations of motion, gained under restrictions from the origin PDE system, are equal to PDEs noted in [28] and [29]. But, there are still solvable by numeric methods, see [30].
If we restrict to small deflections (still fulfilling the restriction of small deformation) we obtain an analytically solvable PDE system. This second restriction is a obvious modification to a real vibrissa compared to the first one. Nevertheless, it is very handy to investigate the qualitative effect of the involved variables.
Then, the displacement $u(s,t)$ and the related derivations are insignificant small due to this restriction of small distractions. As a result, the $x$-component gained by use of the principle of linear momentum is negligible. Furthermore, the deflection $v(s,t)$ can now be described by the inertial-spacial coordinate $x$ instead of the arc length parameter $s$. With respect to relation (1), this leads to the equations:

$$\begin{aligned} s &\rightarrow x \\ u(x,t)\text{and derivatives} &\rightarrow x \\ \varepsilon(x) &= \varepsilon_0(x) = \frac{N_0(x)}{E\,A(x)} \\ \curvearrowright N(x) &= N_0(x) \\ \phi(x,t) &= \partial_x v(x,t) \\ \partial_x \phi(x,t) &= \partial_{xx} v(x,t) \end{aligned}$$

The PDE system then is reduced to the following system of to PDEs:
**Principle of linear momentum: $y$-component**

$$\rho\, A(x)\, \partial_{tt} v(x,t) = \partial_x Q(x,t) + \partial_x \left(N_0(x)\, \partial_x v(x,t)\right) - q\,(x,t)$$

**Principle of angular momentum: $z$-component**

$$0 = \partial_x M(x,t) + Q(x,t)$$

These PDEs can be merged to one PDE (in deriving the derivative of the second PDE wrt. $x$ and solving this for $\partial_x Q(x,t)$). This leads to:

$$\rho\, A(x)\, \partial_{tt} v(x,t) = -\partial_{xx} M(x,t) + \partial_x \left(N_0(x)\, \partial_x v(x,t)\right) - q(x,t)$$

In this paper the effect of axial and distributed loads shall not be investigated, due to [10]. Furthermore, the inner damping of the material is not considered. Therefore the material relation (3) can be simplified to:

$$M(x,t) = E \cdot I_z(x) \cdot \partial_{xx} v(x)$$

This finally formulates the well-known equation of motion:

$$\rho\, A(x)\, \partial_{tt} v(x,t) = -E \cdot \partial_{xx} \left(I_z(x)\, \partial_{xx} v(x,t)\right) \tag{4}$$

This equation of motion (4) is the basis of this paper.

## 2.2. Solution method and discussion

### *2.2.1. Application of the method of separation of variables*

The solution method described in this section is the most used one to investigate the equation of motion of continua vibration. We apply the method of separation of variables to the equations of motion (4). This method provides the reduction of dimensionality of the primary PDE (in case of a sparable PDE). In our case the equation of motion is reduced from a PDE of space and time to one ODE of space and one ODE of time. The conditions for a successfully use of the method of separation of variables are:

- The PDE has to be linear.
- The PDE does not consist of mixed derivatives.
- The coefficients of the partial derivatives are pure functions of the variables the derivative is derived for (or can be converted into).
- The trivial solution $v(x,t) \equiv 0$ can be excluded.

After a successful separation, we get a separate initial- and boundary-value problem if the initial and boundary conditions are also separable, i.e., notable as $t =$ constant and $x =$ constant, respectively. The method of separation of variables supposes that **the solution $v(x,t)$ can be noted as a product of two functions**, each depending on one variable:

$$v(x,t) = X(x) \cdot T(t) \tag{5}$$

Applying the method of separation of variables to (4) yields:

$$\frac{\ddot{T}(t)}{T(t)} = F\{x,\, X(x), \ldots,\, X''''(x)\} = \underline{\kappa}^2.$$

This equation formulates that the left and right hand sides have to be equal for all times and all parts of the beam. This means that they have to be constant. The general complex separation-parameter is denoted by $\underline{\kappa}^2$. There arise two ODEs in $t$ and $x$.

### *2.2.2. The general solution of the time function $T(t)$*

The ODE for $T(t)$ is always the same, i.e., independent of cases of cross-sections and supports of the beam considered here:

$$\ddot{T}(t) - \underline{\kappa}^2\, T(t) = 0\,. \tag{6}$$

The ODE can be classified as a linear, homogeneous ODE of second order. Substitution of $T(t)$ as $e^{\alpha t}$ and using the Euler-Moivre formulas yields the general solution:

$$T(t) = \underline{B}_1\, e^{\underline{\kappa}\, t} + \underline{B}_2\, e^{-\underline{\kappa}\, t} \text{ with } \underline{B}_1,\, \underline{B}_2 \in \mathbb{C}\,. \tag{7}$$

Only the real part $\Re(T(t))$ of the complex function $T(t)$ is of interest. So we split it into an algebraic form:

$$T(t) \quad = \quad e^{\kappa_r\, t} \;\cdot\; (B_{1,r}\, \cos(\kappa_i\, t) - B_{1,i}\, \sin(\kappa_i\, t)) \;+\; e^{-\kappa_r\, t} \;\cdot\; (B_{2,r}\, \cos(\kappa_i\, t) + B_{2,i}\, \sin(\kappa_i\, t)) \tag{8}$$

We conclude from the structure of the solution:

$$\omega \quad = \quad \kappa_i = \text{Im}\,\{\underline{\kappa}\} \tag{9}$$

$$\delta \quad = \quad \kappa_r = \text{Re}\,\{\underline{\kappa}\} \tag{10}$$

The general solution can be adjusted to the cases of vibration in another step. Possible cases of vibration are:

- free, undamped vibrations,
- free, damped vibrations with discrete damping elements,
- forced (un-)damped vibration.

**Example 2.5.** *The adjustment for an important case of the free undamped vibration is shown here. It is well-known that the amplitude of the vibration is bounded for all times. So the solution has to fulfil the condition*

$$0 \not\equiv \lim_{t\to\infty} |T(t)| \leq K$$

*with* $K \in \mathbb{R}_{>0}$, $K < +\infty$. *This condition can only be fulfilled by* $\delta = 0$. *Summarizing we get*

$$T(t) = \widetilde{B}_1 \, \cos(\omega\, t) + \widetilde{B}_2 \, \sin(\omega\, t) \; .$$

*This implies that*

$$\kappa = \kappa_r + i\, \kappa_i = \delta + i\, \omega$$

*and therefore*

$$\underline{\kappa}^2 = -\omega^2 \tag{11}$$

$\kappa^2$ *needs to be real and negative. As usual in common literature (in which nearly exclusive the case of undamped vibration is investigated) the separation parameter is set to* $-\omega^2$ *from the beginning.* ◇

*2.2.3. The general shape solution* $X(x)$

Unlike the general time solution, the general shape solution $X(x)$ can only determined by specification of the cross-area. The solution leads to a system of characteristic parameters: the eigenvalues. The eigenvalues are dependent on the boundary changeover conditions: dependent on the support of the beam. First, the equation of eigenvalues has to be derived. The eigenvalues are directly attached to the separation parameter. Therefore, the variables of interest, i.e., the natural eigenfrequency $\omega$ and the damping coefficient $\delta$, can be determined **after** determination of the eigenvalues under consideration of the boundary conditions.

**Example 2.6.** *Consider a beam with a constant cross-section. The related shape ODE is:*

$$X''''(x) - \underline{\lambda}^4 \, X(x) = 0 \tag{12}$$

*with*

$$\underline{\lambda}^4 := -\frac{\underline{\kappa}^2}{k^4} \, , \qquad k^4 := \frac{E\, I_z}{\rho\, A} . \tag{13}$$

*The general solution is determined by the* $e^{\alpha}$*-ansatz, which yiels:*

$$X(x) = \tilde{\underline{C}}_1 \, \cos(\underline{\lambda}\, x) + \tilde{\underline{C}}_2 \, \sin(\underline{\lambda}\, x) + \tilde{\underline{C}}_3 \, \cosh(\underline{\lambda}\, x) + \tilde{\underline{C}}_4 \, \sinh(\underline{\lambda}\, x)$$

*and in dimensionless form (see Section 3.2.1 for details):*

$$W(s) = \underline{C}_1 \, \cos((\underline{\lambda}\, L)\; s) + \underline{C}_2 \, \sin((\underline{\lambda}\, L)\; s) + \underline{C}_3 \, \cosh((\underline{\lambda}\, L)\; s) + \underline{C}_4 \, \sinh((\underline{\lambda}\, L)\; s) \tag{14}$$

*Finally, we obtain — according to relations* (9) *and* (10) *with substitution* (13)*:*

$$\omega \;\; = \;\; \kappa_i = \mathit{Im}\left\{\underline{\kappa}\right\} = \mathit{Im}\left\{\pm i\, \underline{\lambda}^2\, k^2\right\} \tag{15}$$

$$\delta \;\; = \;\; \kappa_r = \mathit{Re}\left\{\underline{\kappa}\right\} = \mathit{Re}\left\{\pm i\, \underline{\lambda}^2\, k^2\right\} . \tag{16}$$

*An extension of this example in case of no damping leads to (considering relation* (11) *and substitution* (13)*):*

$$\underline{\lambda}^4 = \frac{\omega^2}{k^4} \tag{17}$$

***The eigenvalue*** $\underline{\lambda}$ ***can, in case of no damping, only be real or mere complex (without a real part). Every eigenvalue appears four times****, see exemplarily Fig. 9 for the first (dimensionless) eigenvalue.*

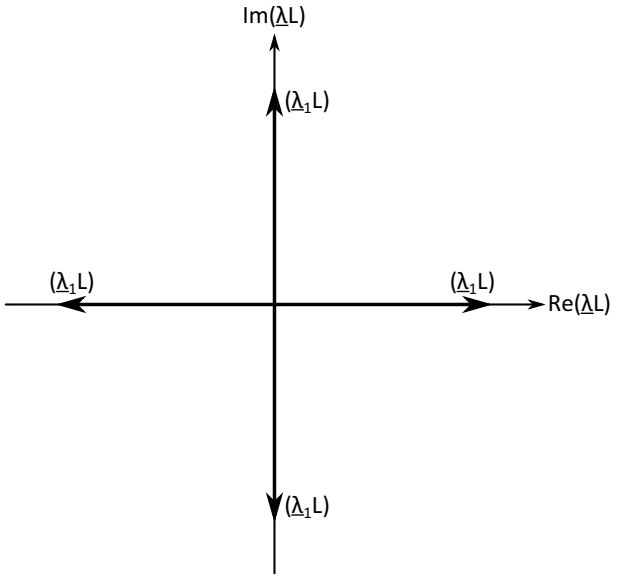


**Fig. 9**. Position of the eigenvalues in the complex plane in case of a cylindrical undamped beam.

◇

## 3. THE CONICAL SHAPED BEAM

### 3.1. Starting point

The conical shape is of particular interest during the investigation of vibrissae. Especially, the ratio of eigenfrequencies from the conical shaped beam to the cylindrical beam is analyzed to show the influence of the conical shape. The following investigations are based on the dynamic beam equation (4) describing beam vibrations. **Let us consider a hollow conically shaped cantilever beam clamped on one side**, see Fig. 10. Further on we assume the following:

- Any influence of damping is negligible;
- The support is realized by a clamping (no viscoelastic support);
- Axial and distributed loads are not considered.

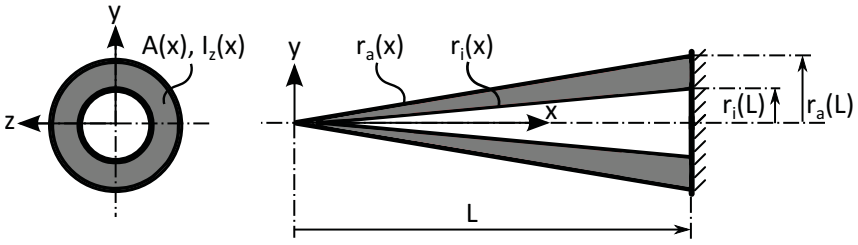


**Fig. 10**. Cross-section of the hollow conically shaped beam

According to Fig. 10

$$\begin{aligned} r_a(x) &= \frac{r_a(L)}{L}\, x =: R_L\, x \\ r_i(x) &= \frac{r_i(L)}{L}\, x = \frac{r_i(L)}{r_a(L)}\, \frac{r_a(L)}{L}\, x =: R_V\, R_L\, x. \end{aligned}$$

the following equations for area and second moment of area can be written as:

$$A(x) = \pi\, R_L^2\, \left(1 - R_V^2\right)\, x^2 \tag{18}$$

$$I_z(x) = \frac{\pi}{4} R_L^4 \left(1 - R_V^2\right) \left(1 + R_V^2\right) x^4 \tag{19}$$

### 3.2. Dynamic beam equation and general solution

The method of separation of variables (5) is used to solve the dynamic beam equation (4). After substitution of the deflection-function in this PDE we have:

$$\frac{\ddot{T}(t)}{T(t)} = -\frac{E}{\rho\, A(x)} \frac{1}{X(x)} \cdot \partial_{xx} \left(I_z(x)\, X''(x)\right) = \underline{\kappa}^2$$

As discussed in Section 2.2.2, the separation generates an ODE for the time-function $T(t)$ which is solved there.

#### *3.2.1. Solution of the shape function $X(x)$*

We have

$$0 = \frac{\rho\,\omega^2}{E} X(x) - \frac{I_z''(x)}{A(x)} X''(x) - 2\,\frac{I_z'(x)}{A(x)} X'''(x) - \frac{I_z(x)}{A(x)} X''''(x)$$

Using (18) and (19) yields:

$$0 = \frac{\rho\,\omega^2}{E\, R_L^2\, (1 + R_V^2)} X(x) - 3\, X''(x) - 2\, x\, X'''(x) - \frac{x^2}{4} X''''(x).$$

For further consideration of boundary conditions it is favorable to convert the ODE for $X(x)$ into a dimensionless type. The following substitutions

$$s := \frac{x}{L} \qquad W(s) := \frac{X(x)}{L}$$

for the dimensionless spatial coordinate $s$ and the deflection $W(s)$ are used. This yields:

$$X^{(n)}(x) = \frac{1}{L^{(n-1)}} W^{(n)}(s)$$

In anticipation to the solution a new eigenvalue $\underline{\gamma}$ is defined:

$$\underline{\gamma}^2 := -\frac{\rho\,\underline{\kappa}^2}{E\, R_L^2 \cdot (1 + R_V^2)} \tag{20}$$

Taking all these relations into account the equation can be written as:

$$0 = \left(\underline{\gamma}\, L\right)^2 W(s) - 3\, W''(s) - 2\, s\, W'''(s) - \frac{s^2}{4} W''''(s)\,. \tag{21}$$

By using a CAS-program like *Maple* the solution is, see also [31], [32] and [33]:

$$W(s) = \frac{1}{s} C_1\, J_2\left(2\sqrt{2\,(\gamma\, L)\; x}\right) + \frac{1}{s} C_2\, Y_2\left(2\sqrt{2\,(\gamma\, L)\; x}\right) + \frac{1}{s} C_3\, J_2\left(2\sqrt{-2\,(\gamma\, L)\; x}\right) + \frac{1}{s} C_4\, Y_2\left(2\sqrt{-2\,(\gamma\, L)\; x}\right) \tag{22}$$

with

$$\begin{aligned} J_n(\cdot) &:= \text{Bessel functions of the first kind, n-th order} \\ Y_n(\cdot) &:= \text{Bessel functions of the second kind, n-th order.} \end{aligned}$$

#### *3.2.2. Characteristic parameters*

With equation (20) together with (9) and (10), the natural eigenfrequency and damping coefficient can be written as:

$$\omega_{kon} = \sqrt{\frac{E\, R_L \cdot (1 + R_V^2)}{\rho\, L^2}} \cdot \mathrm{Im}\left\{\pm i\, \left(\underline{\gamma}\, L\right)\right\} \tag{23}$$

$$\delta_{kon} = \sqrt{\frac{E\,R_L \cdot (1+R_V^2)}{\rho\,L^2}} \cdot \mathrm{Re}\left\{\pm i\ \left(\underline{\gamma}\,L\right)\right\} \tag{24}$$

It should be noted that in contrast to equation (15) and (16) the eigenvalue only appears to the power of one for the conically shaped beam.
Furthermore, in case of no damping, equation (20) becomes — taking (11) into account:

$$\gamma^2 := \frac{\rho\,\omega^2}{E\,R_L^2 \cdot (1+R_V^2)} \tag{25}$$

**Thus the eigenvalues of the conically shaped undamped beam take only real values. Every eigenvalue occurs twice, see Fig. 11.**

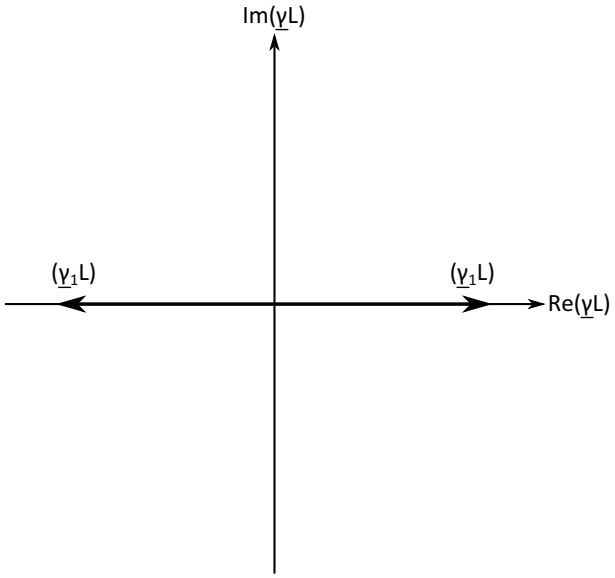


**Fig. 11**. Position of the eigenvalues in the complex plane in case of the conical shaped beam.

### 3.3. Adjustment to the boundary conditions

After determination of the general solution for the shape function for the conical beam in the last section, the adjustment to the boundary conditions has to be made. This leads to an eigenvalue equation from which the characteristic parameters and natural eigenfrequencies are calculated. To pose the boundary conditions the principles of linear and angular momentum are applied to an infinitesimal part of the beam, followed by a limiting process. The dimensionless boundary conditions are:

$$\begin{aligned}
v''(0,t) &= 0 \quad ,\forall t \qquad \rightarrow W''(0) = 0 && (26)\\
v'''(0,t) &= 0 \quad ,\forall t \qquad \rightarrow W'''(0) = 0 && (27)\\
v(L,t) &= 0 \quad ,\forall t \qquad \rightarrow W(1) = 0 && (28)\\
v'(L,t) &= 0 \quad ,\forall t \qquad \rightarrow W'(1) = 0 && (29)
\end{aligned}$$

The consideration of the boundary equations of the general solution (22) gives a linear system of the coefficients from the general solution. Excluding trivial solutions of $W(s)$, the coefficient-matrix has to be singular. The eigenvalue equation then is:

$$\begin{aligned}
&-\sqrt{2}\,J_1\left(2\sqrt{2\,(\gamma\,L)}\right)\,J_1\left(2\sqrt{-2\,(\gamma\,L)}\right)\\
&\qquad+\sqrt{-\,(\gamma\,L)}\,J_1\left(2\sqrt{2\,(\gamma\,L)}\right)\,J_0\left(2\sqrt{-2\,(\gamma\,L)}\right)\\
&\qquad\qquad+\sqrt{(\gamma\,L)}\,J_1\left(2\sqrt{-2\,(\gamma\,L)}\right)\,J_0\left(2\sqrt{2\,(\gamma\,L)}\right)=0.
\end{aligned}$$

### 3.4. Summary of results

Numerical processing of the eigenvalue equation leads to the first five dimensionless eigenvalues:

$$\begin{aligned}(\gamma_1\, L) &= 4.360\\ (\gamma_2\, L) &= 10.573\\ (\gamma_3\, L) &= 19.227\\ (\gamma_4\, L) &= 30.340\\ (\gamma_5\, L) &= 43.917.\end{aligned}$$

- The natural eigenfrequency range
  Due to (25) the natural eigenfrequencies are directly coupled with the calculated eigenvalues. To plot the eigenfrequencies in dependence on the radius and the pitch ratio, $R_V$ and $R_L$, this equation is expanded with $L$ to

$$\omega_n\, p^2 = R_L \sqrt{1 + R_V^2}\; (\gamma_n\, L) \tag{30}$$

  with the material and geometry parameter

$$p^2 := L \sqrt{\frac{\rho}{E}}.$$

  The distribution of the first eigenvalues versus the radius ratio $R_V$ is shown in Fig. 12, where the pitch ratio $R_L$ vary from $0.01$ to $0.1$. A larger pitch ratio is not acceptable, because the beam could no longer be simplified as a slim shear-rigid beam.

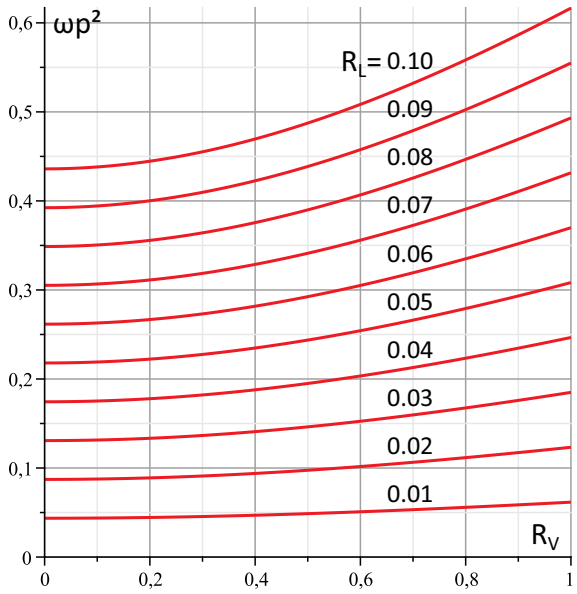


**Fig. 12**. Natural eigenfrequency distribution of the first eigenvalue

- The eigenfrequency ratio
  The ratio of the natural eigenfrequencies of the conical to the cylindrical beam is of particular interest, because the relevance of the conical shape of a vibrissa can be investigated. Therefore, the quotient of (23) and (15) is derived, and this results in (31) for the case of no damping (after back substitution of $R_V$ and $R_L$):

$$\frac{\omega_n}{\omega_{Z,\,n}} = 2\,\frac{(\gamma_n\, L)}{(\lambda_n\, L)^2}\,. \tag{31}$$

  The ratio of the first five eigenfrequencies is shown in Fig. 13.

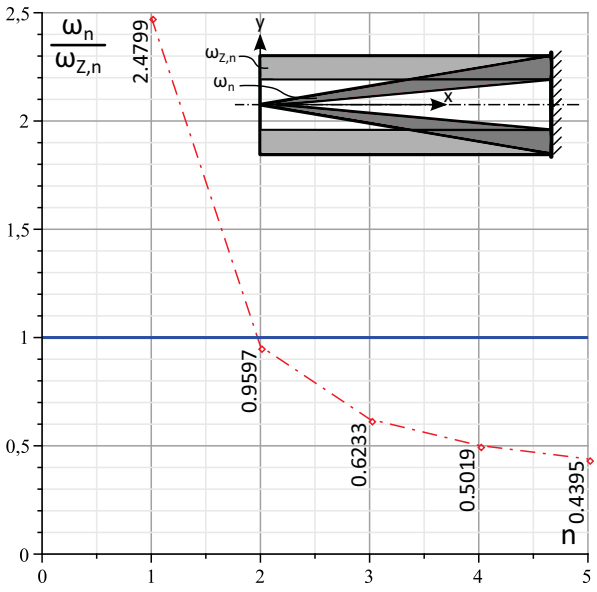


**Fig. 13**. Ratio of the eigenfrequencies of the first five eigenvalues

### 3.5. Discussion of the results

On the basis of the derived relations (30) and (31) as well as on the Figs. 12 and 13 the following results can be concluded.
The equation (30) and Fig. 12, respectively, lead to:

- There exists no local extremum of the natural eigenfrequency $\omega_1$ in dependence on $R_V$ or $R_L$. The global extremum is located at the boundary.
- The natural eigenfrequency $\omega_1$ increases supra-linearly with the radius ratio $R_V$ and with sinking wall thickness, respectively.
- The noted conclusions are also valid for higher eigenfrequencies.

The equation (31) and Fig. 13, respectively, lead to:

- The first eigenfrequency $\omega_1$ of the conically shaped beam is nearly $2.5$-times larger than the eigenfrequency $\omega_{Z.\,1}$ of the cylindrical beam.
- The second eigenfrequency $\omega_2$ stays approximatively the same.
- The ratio of the eigenfrequency $\omega_n$ and $\omega_{Z,\,n}$, $n \geq 2$, is less than $1$ and is decreasing for larger $n$. These trends lead to the conclusion, that the ratio converges to the limit $0$.

**Conclusion 3.1.** *The investigations reveal a growth of the natural eigenfrequencies, especially with shrinking wall thickness. A cupped vibrissa features a higher circular eigenfrequency. Furthermore, the conical shape results in a nearly $2.5$-times magnitude in the first eigenfrequency. This is of particular interest for the active whisker-mode of a vibrissa, because it allows a higher sampling rate which leads to a faster recognition of object shapes and surfaces. Moreover, the conical shape also protects a vibrissa by reducing the stiffness and thus the risk of breakage.*

## 4. A FIRST VIBRISSA MODEL

In this section a first model of the vibrissa with a viscoelastic support (simulating the FSC) is discussed.

### 4.1. Modeling

The following assumptions form the basis of the examination:

- The support elements show linear stiffness and damping behavior.

- Axial forces (may be caused by internal pressure) and distributed loads are not considered.
- The longitudinal elasticity of the supported vibrissa is neglected.
- Limitation on small deflection and deformation of the beam.
- Consideration of narrow beams (Euler-Bernoulli-Beam).
- Restriction of the examination on free (undamped) vibrations with boundary damping in the support.

Figure 14 shows the considered vibrissa model. The selection of this model and the model itself will be briefly discussed in the following.

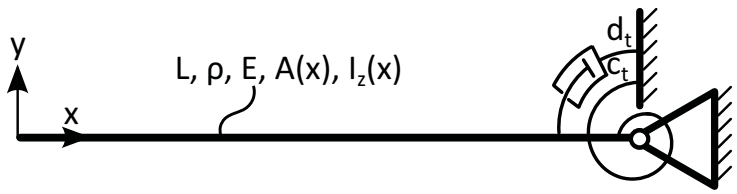


**Fig. 14**. Considered vibrissa model

The selected model is a single vibrissa. The stiffness and damping of the blood sinus is modeled by discrete rotary spring and damper elements at a fixed point at the end of the vibrissa. The validity of this model follows from the fact, that the hair length in the FSC is much shorter then the tactile hair itself. The model has the following benefits:

- The main advantage is the small number of parameters to define the model. The examination will show that only two parameters for the supports stiffness and damping are needed to describe the system. This is of great importance since the analysis will show that the eigenvalues can only be found numerically.
- Another advantage results from the disadvantages of more complex models. In general those models require a sectional description of the beam. For further models see [10].

Two types of beam shapes are being examined in the following:

- cylindrical
- conical, taking the result of Section 3 into account.

### 4.2. The general solution

The mathematical basis of the examination is the differential equation (4). For both considered beam shapes (cylindrical and conical), we get the same ODE for the time $T(t)$. The result of the different differential equations and solutions for the shape function $X(x)$ are two different relations for the eigenfrequency- and for the decay rate.

#### *4.2.1. Modification of the solution $T(t)$*

The general solution (8) was already obtained in Section 2.2.2. In a next step this solution was applied to the case of free undamped oscillations. Because of the rotary damping element in the studied vibrissa model, free oscillation with boundary damping has to be assumed. The solution $T(t)$ has to be modified for this case. It is known that the amplitude of the oscillation decays in time and for $t \to \infty$ fades away, therefore the following constraint applies:

$$\lim_{t\to\infty} T(t) = 0\,.$$

Hence with (8) follows:

$$\begin{cases} B_{1,r} = 0,\ B_{1,i} = 0 & \kappa_r > 0\,, \\ B_{2,r} = 0,\ B_{2,i} = 0 & \kappa_r < 0\,. \end{cases}$$

With the notation $|\delta| := |\kappa_r|$ as the decay constant and $\omega := \kappa_i$ as the eigenfrequency from the relations (9) and (10), we gain the general solution for $T(t)$:

$$T(t) = e^{-|\delta|\,t} \cdot (B_r\,\cos(\omega\,t) + B_i\,\sin(\omega\,t))\,. \tag{32}$$

**Since $\kappa_r$ is not 0 for the damped case, one can no longer conclude that the separation parameter $\underline{\kappa}^2$ is real. Hence complex eigenvalues $\underline{\lambda}$ respectively $\underline{\gamma}$ are to be expected.**

*4.2.2. Solution $X(x)$ and characteristic values*

The solutions for both considered beam shapes have already been found with (14) and (22).
The relations of the eigenfrequency- and the decay rate are gained from the relation (15) for the cylindrical, and relation (16) for the conical beam. It is helpful to define the non-dimensional eigenfrequency and decay constant. The non-dimensional eigenfrequency $\tilde{\omega}$ is directly proportional to the eigenfrequency $\omega$. Likewise, the non-dimensional decay constant $\tilde{\delta}$ is proportional to the decay constant $\delta$. Therefore both values can be used for qualitative analysis on the effect of the support's properties (FSC) without specifying its material and geometry. Further this values can be directly retrieved from the non-dimensional eigenvalues $(\underline{\lambda}\, L)$, respectively $\left(\underline{\gamma}\, L\right)$ calculated before.
For the **cylindrical beam** we get:

$$\tilde{\omega} := \omega \cdot \frac{L^2}{k^2} = \mathrm{Im}\left\{\pm i\ (\underline{\lambda}\, L)^2\right\} \tag{33}$$

$$\tilde{\delta} := \delta \cdot \frac{L^2}{k^2} = \mathrm{Re}\left\{\pm i\ (\underline{\lambda}\, L)^2\right\}. \tag{34}$$

and thus:

$$\tilde{\omega} := \pm\left(\mathrm{Re}\,(\underline{\lambda}\, L)^2 - \mathrm{Im}\,(\underline{\lambda}\, L)^2\right) \tag{35}$$

$$\tilde{\delta} := \pm 2\,\mathrm{Re}\,(\underline{\lambda}\, L)\ \mathrm{Im}\,(\underline{\lambda}\, L) \tag{36}$$

From the relations (35) and (36) follows:

- Generally, the more the non-dimensional eigenvalues $(\underline{\lambda}\, L)$ converge to the angular bisectors of the complex plane, the more the eigenfrequency decreases. Furthermore, it follows that the eigenfrequency is $0$ if the eigenvalue is on the angular bisectors. It will be shown that the interpretation of such an eigenvalue is difficult and remains unclear.
- From the second relation it follows that the absolute value of the decay constant decreases when the non-dimensional eigenvalue converges to the axis of the complex plane. The decay constant is $0$ if the eigenvalue is on the axis of the complex plane. Since only damped oscillation is examined, this case can be excluded.

The location of the non-dimensional eigenvalues in the complex plane for the damped case can be concluded from the relations above. Figure 15 shows an example of the location of the first non-dimensional eigenvalue $\left(\underline{\lambda_1}\, L\right)$. In contrast to the undamped case (see Fig. 9) every eigenvalue exists $8$ times (instead of $4$ times) while every eigenvalue yields the same (non-dimensional) eigenfrequency and decay constant.

Beyond that, another eigenvalue, which is called "0. eigenvalue" in this work, is shown in Fig. 15. This eigenvalue results from the later following numerical analysis. It always exists four times and is located on the angle bisectors. Thus the eigenfrequency of this eigenvalue is $0$.

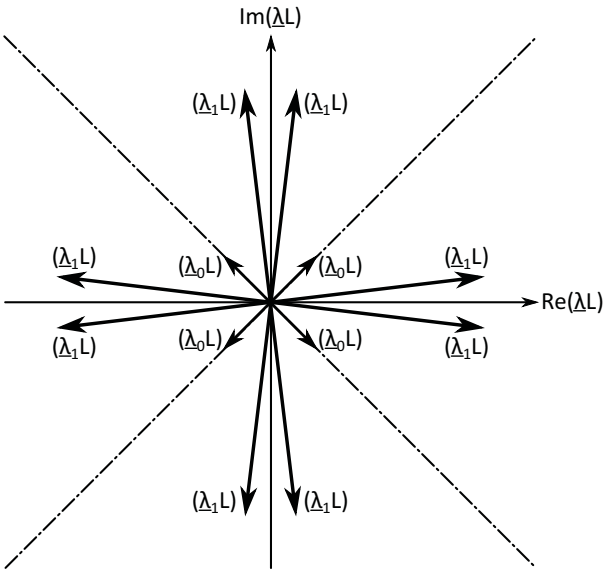


**Fig. 15**. Location of the eigenvalues with boundary damping (cylindrical beam)

In case of the **conical beam** it follows:

$$\tilde{\omega}_{kon} := \omega_{kon} \cdot \zeta = \mathrm{Im}\left\{\pm i \ \left(\underline{\gamma}\, L\right)\right\} \tag{37}$$

$$\tilde{\delta}_{kon} := \delta_{kon} \cdot \zeta = \mathrm{Re}\left\{\pm i \ \left(\underline{\gamma}\, L\right)\right\}. \tag{38}$$

with

$$\zeta = \sqrt{\frac{\rho\, L^2}{E\, R_L \cdot (1 + R_V^2)}}$$

This yields:

$$\tilde{\omega}_{kon} := \mathrm{Re}\left\{\pm \left(\underline{\gamma}\, L\right)\right\} \tag{39}$$

$$\tilde{\delta}_{kon} := \mathrm{Im}\left\{\pm \left(\underline{\gamma}\, L\right)\right\} \tag{40}$$

From the (39) and (40) the following conclusions can be drawn:

- The eigenfrequency does no longer decrease when the eigenvalue converges to the angle bisectors of the complex plane. In fact the eigenfrequency is $0$ in case the eigenvalue is on the imaginary axis.
- For the decay constant we get the inverse relation. The decay constant is $0$ when the eigenvalue is on the real axis of the complex plane.

In contrast to the cylindrical beam, the angle between the two extreme cases is now $90°$ and not $45°$.
As discussed for the cylindrical beam, the location of the non-dimensional eigenvalues in the complex plane and damped case can be concluded for the damped case from the relations above. An example of the location of the first non-dimensional eigenvalue $\left(\underline{\gamma_1}\, L\right)$ is shown in Fig. 16. In contrast to the undamped case every eigenvalue exists $4$ times (instead of 2 times, see Fig. 11). Every eigenvalue of this four yields the same (non-dimensional) eigenfrequency and decay constant.
A "0. eigenvalue" results from the numerical analysis as already explained for the cylindrical beam. This eigenvalue is now on the imaginary axis and exists two times.

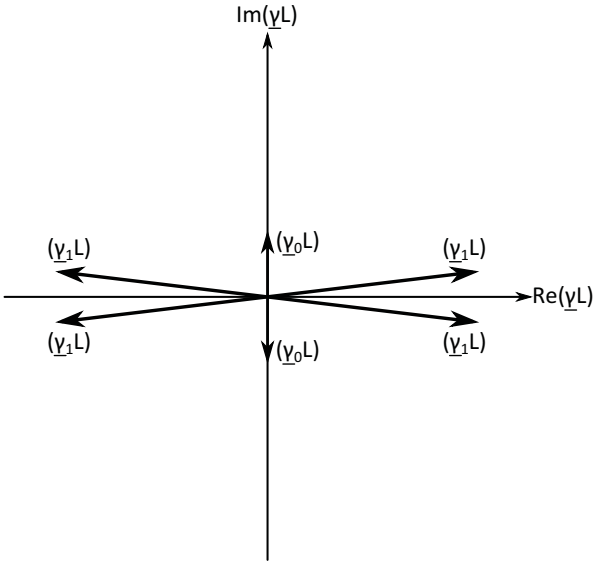


**Fig. 16**. Location of the eigenvalues with boundary damping (conical beam)

Furthermore the **quotient of eigenfrequencies and decay constants** is of interest. The quotient of the eigenfrequency for the conical to the cylindrical beam was already obtained in section 3.4 for the undamped case. Both beams had the same constant ratio of radius. In addition, the outside radius of both beams were the same.
Under this preconditions the **eigenfrequency quotient** can be obtained from the relations (33) and (37). Some further manipulation yield:

$$\frac{\omega_{kon}}{\omega} = 2\,\frac{\tilde{\omega}_{kon}}{\tilde{\omega}} = 2\,\frac{\mathrm{Im}\left\{\pm i \ \left(\underline{\gamma}\, L\right)\right\}}{\mathrm{Im}\left\{\pm i \ \left(\underline{\lambda}\, L\right)^2\right\}}. \tag{41}$$

The obtained relation can be used to verify the later calculated results. The eigenfrequency quotient for high rotary stiffness $c_t$, which comes close to the clamped case, should match the results in Subsection 3.4. Furthermore the examination will show in which way the quotients vary with the support properties.
Since undamped oscillations with boundary damping are considered, the **decay constant quotient** can be found. With the relations (34)) and (38) we get:

$$\frac{\delta_{kon}}{\delta} = 2\,\frac{\tilde{\delta}_{kon}}{\tilde{\delta}} = 2\,\frac{\mathrm{Re}\left\{\pm i\ \left(\underline{\gamma}\,L\right)\right\}}{\mathrm{Re}\left\{\pm i\ \left(\underline{\lambda}\,L\right)^2\right\}}. \tag{42}$$

### 4.3. Formulating the boundary conditions

#### *4.3.1. Damping problem and solution*

To formulate the boundary conditions, an infinitesimal small boundary section has to be cut free. The principles of linear momentum and angular momentum are applied to the element. The following limiting process $dx \to 0$ leads to the boundary conditions which are given by $v(x,t)$ and the related derivatives. In case of no boundary damping there are no derivatives of $T(t)$. Therefore the boundary condition equation can be divided by $T(t) \not\equiv 0$ to gain a boundary condition in $X(x)$ respectively $W(s)$. This boundary condition can directly be used to adapt the general solution of the ordinary DE for $X(x)$ respectively $W(s)$.
If, however, boundary damping exists, derivatives of $T(t)$ will occur beside $T(t)$. Hence $T(t)$ can not be eliminated by division. **For the case of boundary damping the fourth boundary condition (29) exists as an additional differential equation for $\boldsymbol{T(t)}$.** To evaluate the general solution $X(x)$ respectively $W(s)$ an absolute condition in $X(x)$ respectively $W(s)$ is needed.

Two mathematical relations and properties, respectively, will be used to solve this problem.

- The first important relation follows from deriving the general solution (7) of $T(t)$ twice. This yields the following relation:
$$\ddot{T}(t) = \underline{\kappa}^2 \cdot T(t). \tag{43}$$
Thus the solution $T(t)$ reproduces itself with the second derivative.
- The second important property is that a new condition can be gained from a boundary condition (in form of a differential equation) by differentiation.

#### *4.3.2. The boundary conditions*

The first three (non-dimensional) boundary conditions (26), (27) and (28) are independent of the damping and remain the same:

$$\begin{aligned} W''(0) &= 0 \qquad \text{(Free end: moment=0)} \\ W'''(0) &= 0 \qquad \text{(Free end: shear force=0)} \\ W(1) &= 0 \end{aligned}$$

Applying the principle of angular momentum to the right (boundary) damped beam end yields the forth condition:

$$d_t\,\dot{v}'(L,t) + c_t\,v'(L,t) + E\,I_z(L)\,v''(L,t) = 0, \quad \forall t,$$

with $c_t$ as rotary stiffness and $d_t$ as rotary damping constant, see Fig. 14. Applying the method of separation (5) results in:

$$d_t\,X'(L)\cdot\dot{T}(t) + c_t\,X'(L)\cdot T(t) + E\,I_z\,X''(L)\cdot T(t) = 0, \quad \forall t.$$

Considering that a new condition can be gained by differentiating the fourth boundary condition with respect to $t$ (since the fourth boundary condition is a differential equation) yields:

$$\frac{\partial}{\partial t}(\cdot) \;\to\; d_t\,X'(L)\cdot\ddot{T}(t) + c_t\,X'(L)\cdot\dot{T}(t) + E\,I_z(L)\,X''(L)\cdot\dot{T}(t) = 0, \quad \forall t.$$

By considering relation (43) in the new condition, it follows:

$$d_t\,\underline{\kappa}^2\,X'(L)\cdot T(t) + c_t\,X'(L)\cdot\dot{T}(t) + E\,I_z(L)\,X''(L)\cdot\dot{T}(t) = 0, \qquad \forall t.$$

Both conditions can now be combined to one single condition. Some algebraic conversions yield:

$$\left[c_t\, X'(L) + E\, I_z(L)\, X''(L)\right]^2 \cdot T(t) = d_t^2\, \underline{\kappa}^2\, X'(L)^2\, T(t), \qquad \forall t. \tag{44}$$

Due to the previous algebraic expressions, the derivatives of $T(t)$ were eliminated so that the condition could be divided by $T(t) \not\equiv 0$. To evaluate the boundary condition the separation parameter $\underline{\kappa}^2$ has to be substituted by its eigenvalue relation. Hence a distinction of cases for the examined beam shapes is necessary at this point.

- The relation (13) applies to the **cylindrical beam**. Back substitution in (44) finally yields the condition of the form:

$$\left(\alpha_c \mp i\, \left(\underline{\lambda}\, L\right)^2\, \alpha_d\right) \cdot W'(1) + W''(1) = 0, \tag{45}$$

  with the substitutions

$$\alpha_c \;:=\; \frac{c_t}{\frac{E\, I_z}{L}}, \tag{46}$$

$$\alpha_d \;:=\; \frac{d_t}{\sqrt{E\, I_z\, \rho\, A\, L^2}}. \tag{47}$$

  It follows from the substitution that $\alpha_c$ is directly proportional to the support stiffness $c_t$. Furthermore the parameter $\alpha_d$ is directly proportional to the support damping $d_t$. The results show that two parameters are sufficient to describe the vibrissa model. The imaginary unit results from root extraction on both sides.

- For the second case of the **conical beam** equation (20) is needed. Back substitution in (44) and the same procedure finally lead to the following condition:

$$\left(\alpha_c \mp i\, \left(\underline{\gamma}\, L\right)\, \alpha_d\right) \cdot W'(1) + W''(1) = 0 \tag{48}$$

  The parameters $\alpha_c$ and $\alpha_d$ still match the relations (46) and (47). **We note that the non-dimensional eigenvalue $(\boldsymbol{\gamma}\, \boldsymbol{L})$ for the conical shape in relation** (48) **only exists in the first power, in contrast to relation** (45) **of the cylindrical beam**

*4.3.3. Determination of the eigenvector (mode shape)*

The non-dimensional values of the eigenfrequency and decay rate can be obtained directly from the later numerically calculated eigenvalues. Furthermore the related mode shapes are of interest for the then following discussion and analysis of the results. To compute the mode shapes the eigenvector has to be determined. The following remarks concentrate on the evaluation of the eigenvector for the cylindrical beam. The mode shape characteristics of the conical beam can be concluded from the behavior of the mode shape of the cylindrical beam with subject to the parameters $\alpha_c$ and $\alpha_d$.
It is sufficient to consider the first three boundary conditions (26), (27) and (28) to determine the eigenvector since the coefficient matrix is singular. Entering this boundary conditions in the general solution (14) yields:

$$\begin{pmatrix} -1 & 0 & 1 & 0 \\ 0 & -1 & 0 & 1 \\ \cos\left(\underline{\lambda}\, L\right) & \sin\left(\underline{\lambda}\, L\right) & \cosh\left(\underline{\lambda}\, L\right) & \sinh\left(\underline{\lambda}\, L\right) \end{pmatrix} \cdot \vec{\underline{C}} = \vec{0}$$

with

$$\vec{\underline{C}} = \begin{pmatrix} \underline{C}_1 & \underline{C}_2 & \underline{C}_3 & \underline{C}_4 \end{pmatrix}^T.$$

Solving this system for $\underline{C}_4$ we gain:

$$\vec{\underline{C}} = \begin{pmatrix} -\frac{\sin(\underline{\lambda}\, L)+\sinh(\underline{\lambda}\, L)}{\cos(\underline{\lambda}\, L)+\cosh(\underline{\lambda}\, L)} \\ 1 \\ -\frac{\sin(\underline{\lambda}\, L)+\sinh(\underline{\lambda}\, L)}{\cos(\underline{\lambda}\, L)+\cosh(\underline{\lambda}\, L)} \\ 1 \end{pmatrix} \cdot \underline{C}_4.$$

Therefore, the coefficients $\underline{C}_1$, $\underline{C}_2$ and $\underline{C}_3$ of the general solution depend on $\underline{C}_4$.
It makes sense to scale the modal shapes for the figures. Since the left end oft the considered model is free it can be assumed that this free end has the highest amplitude for every mode shape. Division of the found relation by this deflection $W(0)$ delivers the scaled mode shape function:

$$w(s) := \frac{W(s)}{W(0)} = -\frac{1}{2\, \frac{\sin(\underline{\lambda}\, L)+\sinh(\underline{\lambda}\, L)}{\cos(\underline{\lambda}\, L)+\cosh(\underline{\lambda}\, L)}} \cdot \frac{W(s)}{\underline{C}_4}. \tag{49}$$

## 4.4. Solution procedure and presentation of the results

### *4.4.1. Expected solution behavior*

In Section 4.2.2 the expected solution behavior and the location of the eigenvalues with boundary damping was discussed. It was shown that in the case of boundary damping the eigenvalues are no longer on the coordinate axis of the complex plane. This conclusion could be verified by first test calculations.
Afterwards the required boundary conditions were derived in Section 4.3.2. It appeared that a distinction of cases is necessary to gain the fourth boundary condition (45) and (48), respectively. The examination of one case suffices since the multiple eigenvalues are equivalent with respect to the eigenfrequency and the decay constant. The corresponding complex eigenvalues are located in the opposing quadrants.
As expected, the eigenvalues of high support stiffness converge towards the eigenvalues of the clamped beam case. The eigenvalues of low support stiffness and damping converge towards the origin of ordinates that is $0$.

### *4.4.2. The solution procedure*

Considering the boundary conditions in the general solution results in a non-linear complex-valued eigenvalue equation. **Therefore the problem that has to be solved is to find the roots of a non-linear complex-valued equation which can only be solved numerically.**
The computation of the roots can be carried out by declaration of an initial search value. This method can be used if the location of the roots are approximately known. In this case the location is known for high support stiffness. To determine the other complex eigenvalues after variation of the parameters the initial value is adapted successively. This implies that the last found eigenvalue is used as the new initial value for the new search after a variation of the parameter(s).
To gain general conclusions the parameters $\alpha_c$ and $\alpha_d$ were varied in a large range of $10^{-4}$ to $10^4$. It follows that for both cases $\alpha_c = 10^4$ and $\alpha_d = 10^4$, the results are close to the ones of the clamped (undamped) beam.
The search is started with fixed $\alpha_c$, $\alpha_d$ at $\alpha = 10^4$ and the known solution of the clamped beam case for the initial value. In the next step the found solution then is taken as the new initial value to determine the next eigenvalue after decreasing $\alpha_d$. The support stiffness parameter $\alpha_c$ is set to $\alpha_d = 10^4$ after $\alpha_d = 10^{-4}$ and search is restarted. In the same way $\alpha_d$ could be set to a fixed value and $\alpha_c$ is varied from $10^4$ to $10^{-4}$.
The described procedure is successful if the step size of the parameter variation is small enough that the gap from one solution to the next is still small.
For a small range of parameters the 1. eigenvalue and the 0. eigenvalue are close to each other. This makes it difficult to clearly determine the 1. eigenvalue by the explained solution procedure. Therefore the 0. eigenvalue is determined first. It is known that the 0. eigenvalue is located on the angle bisectors, respectively for the conical beam on the imaginary axis. The solutions for the 0. eigenvalue can then be excluded in the search for the 1. eigenvalue. The special case that the 1. eigenvalue is also located on the angle bisectors remains a problem. Maybe the solution is then mistakenly switched. This problem does not exist for the higher eigenvalues in the considered parameter range since the eigenvalues are far away from the angle bisectors respectively from the imaginary axis.
The found eigenvalues are saved in matrices. The parameter $\alpha_c$ is varied in the row and $\alpha_d$ in the column from $10^{-4}$ to $10^4$. **In this work the exponent was varied in 0.5 steps and the results were saved in 17x17-matrices.**

### *4.4.3. Presentation of the results*

In the next section, selected **parts of the results** of the calculations will be gathered. Due to the huge data volume the results will be illustrated graphically.

- The graphics and discussion will focus on the 1. eigenvalue. The higher eigenvalues show the same characteristics with the exception that the corresponding eigenfrequencies are never 0 in the examined parameter range.
- The 0. eigenvalue is not considered here, since no physical interpretation could be found.
- We consider the cylindrical and conical beam shape.

The following explanations facilitate the understanding of the graphical results.

**Cylindrical beam:**

- We examine the second quadrant and determine the non-dimensional eigenvalues which are close to the imaginary axis.

- Grey scale figures are used to illustrate the the non-dimensional eigenfrequency $\tilde{\omega}$ and the non-dimensional decay constant $\tilde{\delta}$. The brightness of a field is directly proportional to the value of the field.
- The corresponding mode shapes are of interest as well. The mode shapes were calculated for 9 fields of the eigenvalue matrix. The calculations were done for the pair of parameters which result for $\alpha_d = 10^{-4}, 10^0, 10^4$ and $\alpha_c = 10^{-4}, 10^0, 10^4$. It will follow that the parameter pairs $(\alpha_d,\, \alpha_c) = \left(10^0, 10^{-4}\right)$ and $(\alpha_d,\, \alpha_c) = \left(10^0, 10^0\right)$ are at high decay constant.

**Conical beam:**

- Instead of the same graphics as in the case of the cylindrical beam, the illustrations are limited to gray-scale graphics which show the eigenfrequency and decay constant quotient.

### 4.5. Numeric evaluation and discussion

#### *4.5.1. The cylindrical beam*

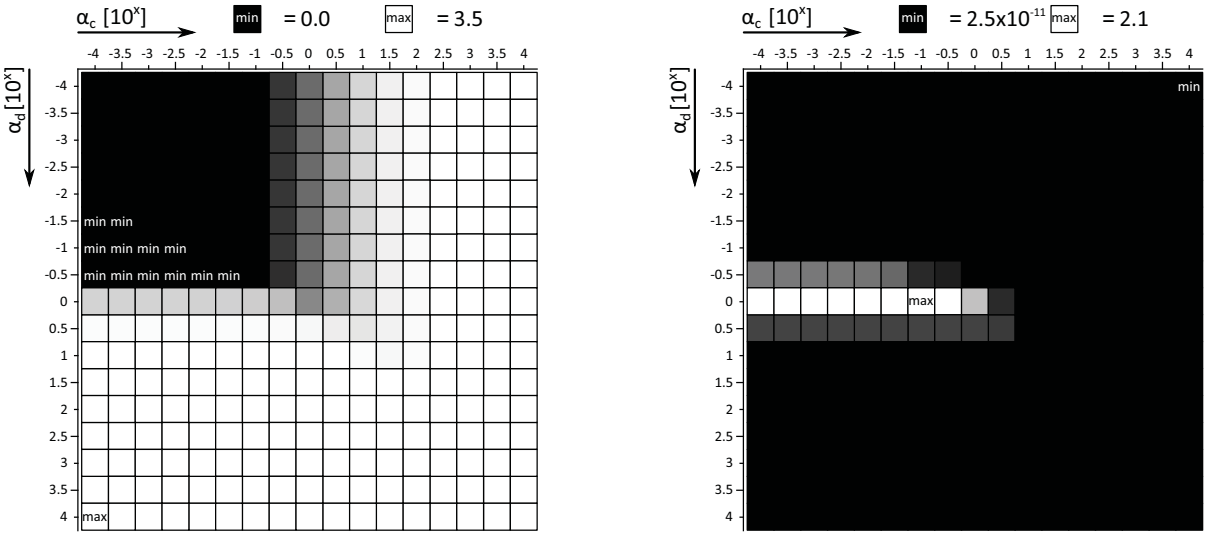


(a) Non-dimensional eigenfrequency

(b) Non-dimensional decay constant

**Fig. 17**. Non-dimensional eigenfrequency and decay constant

The gray-scale plots 17 (a) and 17 (b) yield the following:

- As expected, the viscoelastic support shows the same characteristics as the clamped support with increasing $\alpha_c$. With $\alpha_c \to \infty$ we reach the case of the clamped beam.
- In case of minor $\alpha_c$ and by increasing $\alpha_d$ the support also comes closer to the characteristics of the clamped beam. This stands in contrast to the behavior of the eigenfrequency of a rigid body oscillation. In case of a rigid body oscillation the eigenfrequency would decrease with increasing support damping.
- The eigenfrequency changes only marginally above a certain support damping (for all eigenvalues approximately $\alpha_d = 10^0$) respectively a support stiffness (for all eigenvalues approximately $\alpha_c = 10^2$). Beyond this range the eigenfrequency even increases minimally with decreasing stiffness respectively damping. This is in sharp contrast to a damped rigid body oscillation.
- The eigenfrequency varies the most below this support stiffness and damping range.
- **For a certain set of parameter pairs (black, min) the eigenfrequency is even 0.**
- The highest variation of the eigenfrequency corresponds with the support damping parameters of the highest decay constant. The drop of the eigenfrequency to 0, is obviously at the maximum decay constant.
- The maximum eigenfrequency is in the column of the lowest and not as expected in the column of the highest support stiffness. This effect is only noticeable at the forth decimal place.

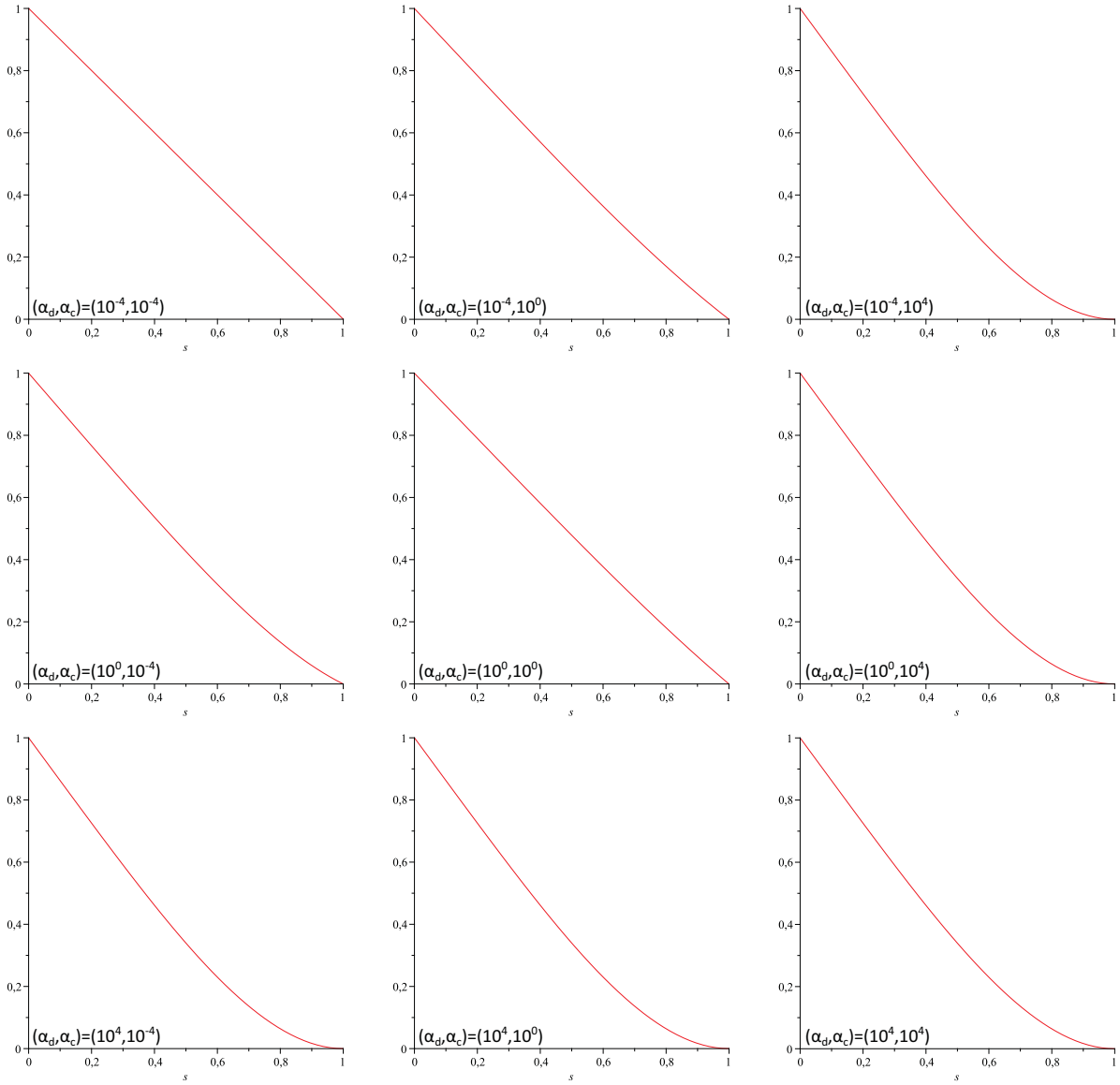


**Fig. 18**. Mode shapes for the different pairs of parameters

From the mode shape presentation, see Fig. 18, we gain the following:

- Low support stiffness and damping yields mode shapes which are close to the mode shapes of a beam with a thrust bearing on one side without support damping and stiffness.
- High stiffness or damping in the support results in mode shapes which are close to those of a clamped beam. Hence, the slope of the beam at the support tends towards 0.
- The mode shape is similar to the one of the clamped beam until the maximum decay constant is reached. Beyond this support damping, the mode shape converges to the mode shape of a beam with a thrust bearing on one side.

**Conclusion 4.1.** *The results show that the eigenfrequency behavior of a beam with a pivot bearing on one side and boundary damping is contrary to the behavior of the damped rigid body model. The eigenfrequency decreases with decreasing support stiffness for a rigid body model. For the examined model it follows that the eigenfrequency increases marginally by decreasing support stiffness beyond a certain support damping. Furthermore it is known that the eigenfrequency decreases for increasing damping for a rigid body oscillation. In contrast the results of the examined model show that the eigenfrequency increases with the support damping.*
*The distinctiveness of the 1. eigenvalue in the examined range of parameters is based on the fact, that the eigenfrequency amounts to 0 for certain parameter pairs. The interpretation of this remains unclear. A boundary point*

*with the angle bisector would have been conceivable: for a set of one pair of parameters, a kind of aperiodic boundary case for which the wave reflexion is tuned in a way that the standing wave slowly converge to the position of rest, could be expected. However, why the eigenfrequency is 0 for a range of parameters and furthermore shows a discontinuous behavior depending on the support damping can still not be explained.*

*4.5.2. The conical beam*

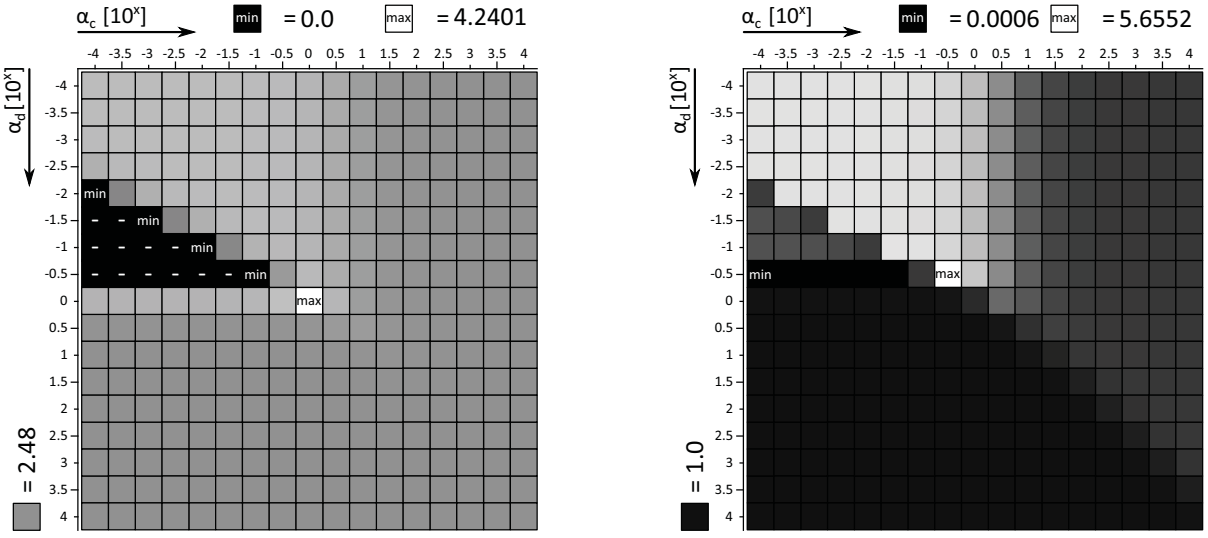


(a) Ratio of the eigenfrequency

(b) Ratio of the decay constant

**Fig. 19**. Ratio of eigenfrequency and decay constant (conical/cylindrical)

From the gray-scale plot of the eigenfrequency quotient (Fig. 19 (a)) we gain:

- The results for the eigenfrequency quotient, obtained in Section 3.4, could be confirmed by the calculations in this section.
- It followed, that the ratio is almost constant on a large range of parameters.
- **With $\alpha_c = 10^0$ and $\alpha_d = 10^0$ follows a local maximum of the eigenfrequency.**
- For the parameter pairs for which the eigenfrequency is $0$ (cylindrical beam), the quotient could not be determined.

The gray-scale plot for the decay constant quotient (Fig. 19 (b)) yields:

- The gray-scale plot is divided into three areas in which the quotient is almost constant.
- The quotient is approximately $1$ for a large range of high damping in the support.
- In the field of evanescent eigenfrequency, the quotient converges towards 0 ($\alpha_d = 10^{-0.5}$). The same support stiffness and $\alpha_c = 10^{-0.5}$ however yields the maximum of the quotient of the eigenfrequency.

**Conclusion 4.2.** *These results confirm the findings of Section 3.4. In addition they show that the eigenfrequency quotient depends on the support parameters. The support stiffness and damping edges which were discussed for the cylindrical beam also appear in the quotients of the eigenfrequency and decay constants. This edges divide the gray-scale into several ranges with almost constant ratio. What might be the importance of this ratios regarding the biological vibrissae remains to be examined.*

*4.5.3. Interpretation of the results with respect to a possible technical realization*

The primary goals of a technical sensory system realizing the active mode of the vibrissa are:

- high sampling rate (high eigenfrequency),

- high sensitivity, that is sufficient support compliance,
- good controllability of the active mode that is fast turning-on and -off.

Figure 19 is of particular importance for the interpretation. The figure yields that the eigenfrequency generally decreases by decreasing support stiffness and damping. On the other hand $\alpha_c = 10^0$ and $\alpha_d = 10^0$ mark a special point. At this point the eigenfrequency is still high due to the maximum of the eigenfrequency quotient of both considered beam shapes. Furthermore this point of support parameters is far away from the case of the clamped beam. Therefore a high sensitivity can be expected. As a result of this location of the support parameters small variation of the support properties suffice to steer into the highly damped range. In this range the vibrissa oscillation decays fast.**Therefore the point of support parameters $\alpha_c = 10^0$ and $\alpha_d = 10^0$ marks an interesting operating point with respect to the technical realization.** Whether this point is of importance for the real vibrissa (maybe it is an operating point of the vibrissa), this has to be analyzed in further examinations.

## 5. SUMMARY AND FUTURE PROSPECTS

The goal of this paper was to present the theoretical context needed to examine the mechanical and in particular the dynamical characteristics of the biological vibrissa. Moreover these theoretical aspects were to be interpreted with respect to the biological vibrissa, as well as for a technical implementation of it. The focus of the studies lay on the examination of the influence the compliance of the tactile hair, its viscoelastic support and its conical form have on the oscillation characteristics of the vibrissa.
As a first step the differential equations of the oscillation were derived for a standardized biological vibrissa (elastic, conical beam), hence allowing great deflections and displacements, while assuming small deformations of the beam. The theoretical examinations on the conical shape of the beam confirmed the observation that its eigenfrequencies grow when the conical gradient increases, as this leads to a greater bending stiffness. Furthermore it has been shown that the eigenfrequencies also grow with decreasing wall thickness (or increasing ratio of the inner- to the outer-radius) and reach their minimum for the full cross-section. These findings confirm the importance of the conical form of the vibrissa, since only high eigenfrequencies allow a high resolution of the information to be gathered on the examined surface.
Further on the influence of the viscoelastic support of the vibrissa has been examined using an abstract model in which the vibrissa was modeled as a thin, flexible beam having either a constant or a tapered shape. The viscoelastic properties of the FSC were implemented by using torsional spring and damping elements at the center of rotation. The damping element significantly increased the complexity of the differential equations and led to two surprising phenomenons:

- The first eigenfrequency was $0$ for a certain range of parameters.
- Another ”$0$. eigenvalue” appeared which eigenfrequency was always $0$.

Why this happens and above all, what physical interpretations could apply for this behavior, is still unclear.
However the study demonstrated that the oscillation behavior of an elastic beam differs remarkably from the behavior of a rigid body:

- The eigenfrequencies increase with growing boundary damping.
- For specific damping parameter values, the eigenfrequencies grow for decreasing boundary stiffness.
- A local maximum exists for the decay constant depending on the support damping.
- The amplitude of the decay constant decreases with increasing boundary stiffness.

The ratio of eigenfrequency and the decay constant were calculated for the case of the conical beam. The results confirmed the results which were gained for the clamped conical beam. In addition these calculations yield that the quotients depend on the support parameters. The quotient of the decay constant was about $1$ for one third of the examined parameter range. The shape of the gray-scale plot of the eigenfrequency of the cylindrical beam could also be found in the gray-scale plot of the eigenfrequency quotient. The importance of the conical shape was discussed in respect to the technical implementation. It followed that the support operating point $\alpha_c = 10^0$ and $\alpha_d = 10^0$ is of special importance regarding the prerequisites (high sampling rate, high sensitivity, high controllability).

## 6. ACKNOWLEDGEMENT

The authors thank Prof. rer. nat. habil. (em.) Joachim Steigenberger (Ilmenau) for fruitful discussions, hints and continuous interest.

## 7. REFERENCES

[1] Tae-Eun Jin, Veit Witzemann, and Michael Brecht, "Fiber types of the intrinsic whisker muscle and whisking behavior," *The Journal of Neuroscience*, vol. 24, no. 13, pp. 3386–3393, 2004.

[2] M. Wichmann, "http://www.flickr.com/photos/m2w2/3712187953/sizes/ovin/photostream/," (15.01.2011).

[3] W. Scott, "http://www.wormsandgermsblog.com/articles/animals/pocket-pets/," (15.01.2011).

[4] K. Carl, *Technische Biologie des Tasthaar-Sinnessystems als Gestaltungsgrundlage für taktile stiftführende Mechanosensoren*, Dissertation, TU Ilmenau, 2008.

[5] J. Dörfl, "The musculature of the mystacial vibrissae of the white mouse," *J. Anat.*, vol. 135, pp. 147–154, 1982.

[6] A. Schierloh, *Neuronale Netzwerke und deren Plastizität im Barrel-Kortex der Ratte.*, Ph.D. thesis, Technische Universität München, Fakultät Wissenschaftszentrum Weihenstephan für Ernährung, Landnutzung und Umwelt, 2003.

[7] T.A. Schmitz, "Modellbildung des Reizleitungsapparates am Beispiel Vibrisse und adaptive Regelungsprozesse.," 2009.

[8] M. J. Hartmann and J. H. Solomon, "Robotic whiskers used to sense features : Whiskers mimicking those of seals or rats might be useful for underwater tracking or tactile exploration.," *NATURE*, vol. 443, pp. 525, 2006.

[9] T.A. Schmitz, "Entwurf und Analyse von biologisch inspirierten Sensorsystemen mit erhöhtem Freiheitsgrad am Beispiel Vibrisse.," M.S. thesis, TU Ilmenau, 2011.

[10] M. Schäfer, "Beiträge zur Theorie der Balkenschwingungen mit Anwendungen in der biologisch inspirierten Robotik/Sensorik.," 2011.

[11] B. Mitchinson, K.N. Gurney, P. Redgrave, C. Melhuish, A.G. Pipe, M. Pearson, I Gilhespy, and T.J. Prescott, "Empirically inspired simulated electro-mechanical model of the rat mystacial follicle-sinus complex," *Proc. R. Soc. Lond.*, vol. 271, pp. 2509–2516, 2004.

[12] B. Mitchinson, C.J. Martin, R.A. Grant, and T.J. Prescott, "Feedback control in active sensing: rat exploratory whisking is modulated by environmental contact," *Proc. R. Soc. B*, vol. 274, pp. 1035–1041, 2007.

[13] R.W. Berg and D. Kleinfeld, "Rhythmic whisking by rat: Retraction as well as protraction of the vibrissae is under active muscular control," *Journal of Neurophysiology*, vol. 89, pp. 104–117, 2003.

[14] D. Hill, R. Bermejo, P. Zeigler, and D. Kleinfeld, "Biomechanics of the vibrissa motor plant in rat: Rhythmic whisking consists of triphasic neuromuscular activity," *The Journal of Neuroscience*, vol. 28, pp. 3438–3455, 2008.

[15] C. Behn, *Ein Beitrag zur adaptiven Regelung technischer Systeme nach biologischem Vorbild.*, Ph.D. thesis, TU Ilmenau, 2005.

[16] C. Behn, J. Steigenberger, and K. Zimmermann, "Finite degree-of-freedom models for animal vibrissae," *ECC 2009,Budapest*, pp. 2500–2505, 2009.

[17] C. Behn and J. Steigenberger, *Improved Adaptive Controllers For Sensory Systems - First Attempts, in Modeling, Simulation and Control of Nonlinear Engineering Dynamical Systems*, Number ISBN 978-1-4020-8777-6. Springer, 2009.

[18] A. Birdwell, J. Solomon, M. Thajchayapong, M. Taylor, M. Cheely, R. Towal, J. Conradt, and M. Hartmann, "Biomechanical models for radial distance determination by the rat vibrissal system," *The Journal of Neurophysiology*, vol. 98, pp. 2439–2455, 2007.

[19] G. Scholz and C. Rahn, "Profile sensing with an actuated whisker," *IEEE Transactions on Robotics and Automation*, vol. 20, pp. 124–127, 2004.

[20] M.A. Neimark, M.L. Andermann, J.J. Hopfield, and C.I. Moore, "Vibrissa resonance as a transduction mechanism for tactile encoding," *The Journal of Neuroscience*, vol. 23(16), pp. 6499–6509, 2003.

[21] M.L. Andermann, J. Ritt, M. Neimark, and C.I. Moore, "Neural correlates of vibrissa resonance: Band-pass and somatotopic representation of high-frequency stimuli," *Neuron*, vol. 42, pp. 451–463, 2004.

[22] H. Irretier, *Grundlagen der Schwingungstechnik 2 : Systeme mit mehreren Freiheitsgraden, Kontinuierliche Systeme.*, Friedr. Vieweg & Sohn Verlagsgesellschaft mbH, 2001.

[23] D. Gross, W. Hauger, W Schnell, and P. Wriggers, *Technische Mechanik : Band 4 Hydromechanik, Elemente der Hoeheren Mechanik, Numerische Methoden.*, Springer-Verlag, 4 edition, 2002.

[24] M. Géradin and Rixen D., *Mechanical Vibrations: Theory and Application to Structural Dynamics.*, John Wiley & Sons Inc., 1997.

[25] W. Weaver, S. P. Timoshenko, and D. H. Young, *Vibration Problems in Engineering.*, John Wiley & Sons Inc., 5 edition, 1990.

[26] R. Hinrichs, *Gedämpfte Schwingungen vorgespannter Balken.*, VDI-Verlag Gmb, 1990.

[27] S. Krenk, *Mechanics and Analysis of Beams, Coloums and Cables.*, Springer-Verlag, 2 edition, 2001.

[28] S. R. Woodall, "On the large amplitude oscillations of a thin elastic beam.," *Int. J. Non-linear Mechanics*, vol. 1, pp. 217–238, 1966.

[29] S. Wojciech, "Nonlinear vibration of a simply supported, viscoelastic inextensible beam and comparison of four methods.," *Acta Mechanica*, vol. 85, pp. 43–54, 1990.

[30] A. Pielorz, "Nonlinear equations for a thin beam.," *Acta Mechanica, published online: Springer-Verlag 2003*, 2003.

[31] G. Kirchhoff, "Über die Transversalschwingungen eines Stabes von veränderlichem Querschnitt," *Monatsberichte der Kniglich Preuischen Akademie der Wissenschaften zu Berlin*, vol. (zur: Sitzung der phys.-math. Klasse vom 27. October 1879), pp. 815–828, 1879.

[32] R.P. Goel, "Transverse vibrations of tapered beams," *Journal of Sound and Vibration*, vol. 47(1), pp. 1–7, 1976.

[33] S. Naguleswaran, "A direct solution for the transverse vibration of euler-bernoulli wedge and cone beams.," *ournal of Sound and Vibration*, vol. 172(2), pp. 289–304, 1994.